JOURNAL OF GUIDANCE, CONTROL, AND DYNAMICS
Vol. 32, No. 6, November–December 2009

Dynamics of Towed Payload System Using Multiple Fixed-Wing Aircraft

Paul Williams* and Wubbo Ockels†
Delft University of Technology, 2629 HS Delft, The Netherlands

DOI: 10.2514/1.44371

The payload capability of many aircraft is typically limited by the maximum takeoff weight. However, when in flight, many aircraft can handle larger loads, but this capability is rarely exploited. The possibility of using an aircraft cable system to lift large payloads is studied in this paper. This concept has been studied previously for single-aircraft, single-cable systems in some detail. The major limitation of such systems is the need to fly very tight circles at high-lift coefficients. This limits the size of the payload that can be retrieved with such a system. To overcome this, it is possible to employ a multiple-aircraft, multiple-cable system to allow greater control of the payload position as well as allowing a much wider choice of aircraft speed and lift coefficient. In this paper, an object-oriented cable modeling approach is used to study the relative equilibria of such a system. Parametric studies of different payload masses and aircraft orbit parameters are presented, and the dynamic stability is analyzed. Collision-free transition trajectories that take the multiple-aircraft system from circular flight into straight and level flight are derived.

I. Introduction

THE possibility of performing remote payload pickup and delivery using long cables towed by fixed-wing aircraft has received attention in the technical literature for several decades. In fact, the possibilities were developed conceptually as early as the 1930s [1,2] and were rediscovered in the 1940s [3] by the missionary pilot, Nate Saint, who used the technique to deliver small items to remote regions in Ecuador [4] (see [5] for a photograph of the technique). These and other documented concepts and applications [6,7] are concerned with using a single aircraft flying constant radius circles with a tether deployed to the ground. For certain combinations of aircraft orbital parameters and cable parameters, the cable takes on a stable relative equilibrium configuration (relative to a rotating frame) with the orbit radius of the cable tip very small compared to the aircraft orbit radius. This translates to nearly stationary motion in the inertial frame, depending on the aircraft angular velocity.

The stability of so-called circularly towed-cable systems has received considerable focus [8–16]. Much of the earlier work on such systems has focused on multivalued solutions at high angular velocities. However, many of these high-angular-velocity solutions are not relevant to aircraft-towed systems due to the relatively low angular velocities and longer cables involved. Therefore, more recent effort has studied optimal configurations and ways of enhancing the near-stationary motion of the cable tip [17]. Williams and Trivailo [18] also studied the dynamics of the cable during aircraft transition maneuvers and showed that the aircraft transition from straight flight to circular flight can have a significant influence on the cable dynamics. Periodic solutions of a single-cable towed system for vertical aircraft oscillations, elliptic orbits, and crosswinds were presented in [19]. Periodic optimal solutions including cable winch control in the presence of crosswinds were determined in [20] using direct transcription methods. A method for delivering payloads to the ground or ocean was studied in [21] by anchoring the cable tip and sliding the payloads on the cable. Control of the aircraft motion for stabilizing wind-induced oscillations of a circularly towed-cable system (for the E-6A TACAMO) using fuzzy logic was presented by Borst et al. [22] and Brushwood et al. [23].

The conventional circularly towed-cable system is based on the idea of using a single aircraft with a single towed cable. The major problem with such a system is that, when the mass at the cable tip increases, there is a significant change in the equilibrium condition, which causes the orbit radius of the cable tip to increase. Hence, the desired near-stationary motion is lost. The most important consequence of this is when it is desired to deliver the payload to an alternative location using the same physical principles. It would not be possible to initiate the near-stationary motion with such a large mass. Another significant drawback is that the required aircraft orbit parameters to maintain the desired cable tip motion are at the extremes of the aircraft operational envelope, that is, maximum lift coefficient and bank angle. The increase in cable tension due to the increased load could then stall the aircraft, thereby severely restricting the range of operation of the system. It must be noted that the original system used by Nate Saint involved only lightweight payloads.

An alternative technique that was originally suggested by Alabrune [24,25] is to use two or more aircraft to retrieve a payload by using a similar technique as just described, but connecting the same payload to more than one tow cable, as shown in Fig. 1. In the case of a two-aircraft system, the aircraft would fly at diametrically opposite sides of the circle (spaced 180 deg apart) so that the cable tips approach the center of the circle. At this point, the cables can be connected to the payload. The advantage of this technique over the single-line method is that the components of cable tension acting to pull the payload away from the center of the circle is ideally balanced by the second cable. Hence, the new equilibrium position is with the payload at the exact center of the circle, with zero inertial velocity. Naturally, this technique extends to multiple-aircraft and multiple cables. Alabrune [24,25] discussed techniques for maneuvering the aircraft to raise the payload from the ground. Essentially, he suggested accelerating one of the aircraft relative to the other. Wilson [26] proposed different procedures for the "tow-in" and "tow-out" maneuvers using the two-aircraft configuration.

Despite the considerable apparent value in developing a multi-aircraft cable pickup system, there is no publicly available technical literature that studies the dynamics of multicable systems for vertical pickup and delivery of payloads. This paper seeks to fill this void by developing an object-oriented mathematical model for dealing with the multicable dynamics and using the model to assess the stability of the system under a variety of operating conditions. The model is used

Presented as Paper 6375 at the AIAA Atmospheric Flight Mechanics Conference, Keystone, CO, 21–24 August 2006; received 14 March 2009; revision received 23 June 2009; accepted for publication 7 July 2009.

*Applied Researcher, Faculty of Aerospace Engineering; tethered.systems@gmail.com. AIAA Member.

†Aerospace Sustainable Engineering and Technology Chairholder, Faculty of Aerospace Engineering, Postbus 5058; w.j.ockels@tudelft.nl.

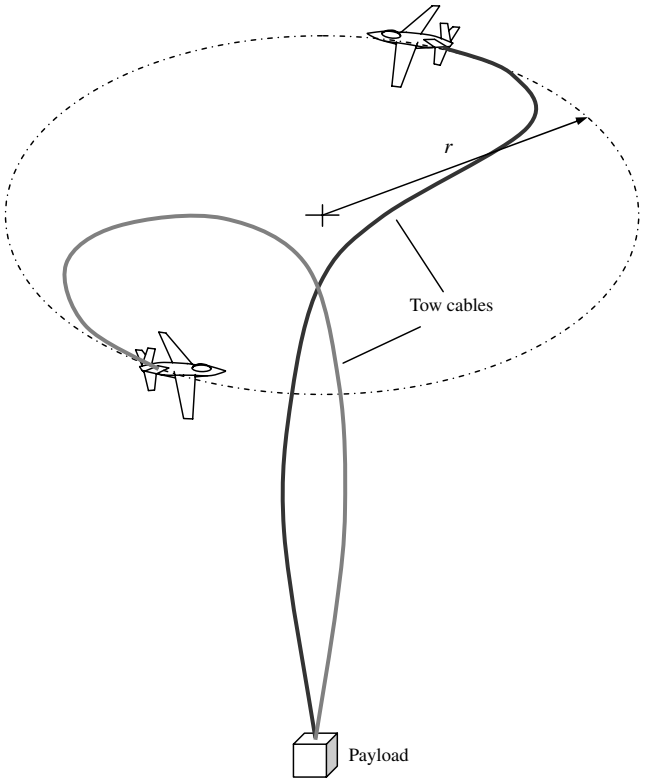

Fig. 1 Vertical payload pickup using multiple towed cables.

to study the transient dynamics of the system during crosswinds and gusts, errors in aircraft position, removal of payload mass, and payload lifting. In particular, transition from circular flight to straight flight is presented using a trajectory generation technique developed specifically for the transition maneuver. Preliminary assessment of nonpoint mass payloads is performed using simplified rigid-body payload models. This work is intended to serve as a basis for more detailed design leading to practical implementation. This paper is limited to a study of the system dynamics and hence does not present a detailed analysis of operational concepts.

II. Multiple Circularly Towed-Cable Model

The dynamics of towed-cable systems have been studied using a variety of different modeling techniques. These range from continuous models discretized using an assumed-modes-type technique [13,14] to discrete lumped parameter models [17]. In this paper, the lumped mass model is chosen because of its relative simplicity and the ease with which it can be adapted for equilibrium analysis and transient dynamic studies. Lumped mass models of cable dynamics were used in [17–20] to study both the stability and dynamic behavior of a single towed-cable system. To conduct a stability analysis, it is preferable to use a rotating coordinate system that rotates with the angular velocity of the aircraft so that the relative cable equilibria appear as stationary motion in the rotational coordinates. To efficiently deal with a multicable system, an object-oriented approach is used whereby a single-cable entity is constructed that treats each cable and end body as a single object. The coupling between the different cable objects is handled by additional external forces acting on the end body.

A. Single-Cable Model in Rotating Coordinate Frame

To describe the dynamics of the multiple-cable system, we begin with the dynamics of a single cable and extend this to the general multiple-cable case. The coordinate system used in this paper is attached to the center of the aircraft's nominal orbit at position O, as shown in Fig. 2. The unit vectors describing the coordinate directions are denoted by $(\mathbf{x}_1, \mathbf{x}_2, \mathbf{x}_3)$. The inertial axes, also centered at O, are

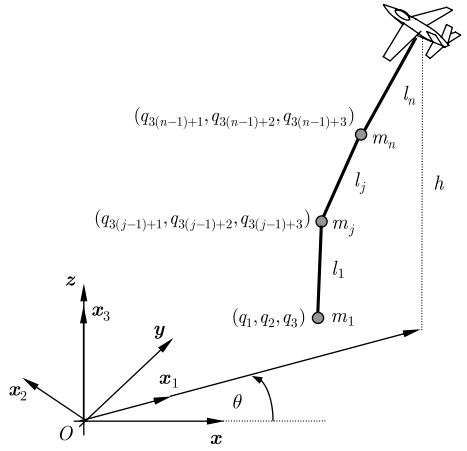

Fig. 2 Lumped mass model for a single cable.

denoted by $(\mathbf{x}, \mathbf{y}, \mathbf{z})$. The position of the jth mass in the rotating coordinates is given by

$$\mathbf{r}_j = q_{3(j-1)+1}\mathbf{x}_1 + q_{3(j-1)+2}\mathbf{x}_2 + q_{3(j-1)+3}\mathbf{x}_3, \qquad j = 1, \ldots, n \quad (1)$$

where $(q_{3(j-1)+1}, q_{3(j-1)+2}, q_{3(j-1)+3})$ describes the Cartesian position of the jth mass in the rotating frame. Note that the cable elements are numbered from one at the payload through to n at the aircraft end. The numbering of the coordinates is used to enable a straightforward implementation of the equations of motion in a simulation environment (i.e., single state vector), and the payload is numbered one to allow for varying the number of deployed cable elements easily from the aircraft end (i.e., cable deployment). The inertial velocity expressed in the rotating coordinate frame is obtained as

$$\mathbf{v}_j = (\dot{q}_{3(j-1)+1} - \dot{\theta} q_{3(j-1)+2})\mathbf{x}_1 + (\dot{q}_{3(j-1)+2} + \dot{\theta} q_{3(j-1)+1})\mathbf{x}_2 + \dot{q}_{3(j-1)+3}\mathbf{x}_3, \qquad j = 1, \ldots, n \quad (2)$$

where $\dot{\theta} = v/r$ is the angular velocity of the aircraft in the circular orbit, v is the nominal aircraft velocity, and r is the nominal aircraft orbit radius. We assume that $\dot{\theta}$ is constant in the reference model. However, nonuniform angular motion can also be simulated using this reference system, as will be described in a later section. Differentiating Eq. (2) gives the inertial acceleration of the jth mass in the rotating frame as

$$\mathbf{a}_j = (\ddot{q}_{3(j-1)+1} - 2\dot{\theta}\dot{q}_{3(j-1)+2} - \dot{\theta}^2 q_{3(j-1)+1})\mathbf{x}_1 + (\ddot{q}_{3(j-1)+2} + 2\dot{\theta}\dot{q}_{3(j-1)+1} - \dot{\theta}^2 q_{3(j-1)+2})\mathbf{x}_2 + \ddot{q}_{3(j-1)+3}\mathbf{x}_3, \qquad j = 1, \ldots, n \quad (3)$$

Note that Eqs. (1–3) apply regardless of the selected cable object. The specific cable is dictated by the position of the aircraft, which alters the boundary conditions for application of the tension in the nth cable element.

It is relatively straightforward to write the equations of motion using Newton's second law as

$$\mathbf{a}_j = \frac{\mathbf{F}_j^s + \mathbf{F}_j^d + \mathbf{F}_j^g + \mathbf{F}_j^a}{m_j}, \qquad j = 1, \ldots, n \quad (4)$$

where m_j is the mass of the jth cable element, given by

$$m_j = \begin{cases} m_p + \frac{\rho_c}{2} L_{s_1} & j = 1 \\ \frac{\rho_c}{2}(L_{s_{j-1}} + L_{s_j}) & j = 2, \ldots, n \end{cases} \quad (5)$$

ρ_c is the cable mass density per unit length, m_p is the mass of the payload at the end of the cable, and L_{s_j} is the unstrained length of the jth cable element.

Using Eq. (3), we obtain

$$\ddot{q}_{3(j-1)+1} = 2\dot{\theta}\dot{q}_{3(j-1)+2} + \dot{\theta}^2 q_{3(j-1)+1} + (\mathbf{F}_j^s + \mathbf{F}_j^d + \mathbf{F}_j^g + \mathbf{F}_j^a) \cdot \mathbf{x}_1/m_j$$

$$\ddot{q}_{3(j-1)+2} = -2\dot{\theta}\dot{q}_{3(j-1)+1} + \dot{\theta}^2 q_{3(j-1)+2} + (\mathbf{F}_j^s + \mathbf{F}_j^d + \mathbf{F}_j^g + \mathbf{F}_j^a) \cdot \mathbf{x}_2/m_j$$

$$j = 1, \ldots, n \qquad \ddot{q}_{3(j-1)+3} = (\mathbf{F}_j^s + \mathbf{F}_j^d + \mathbf{F}_j^g + \mathbf{F}_j^a) \cdot \mathbf{x}_3/m_j \quad (6)$$

There are a number of important forces that appear in the right-hand side of Eqs. (4) and (6). The most important that are considered in this work are tension/spring s, internal damping d, gravity g, and aerodynamic a. Each of these forces is described in Appendix A. For better scaling, all lengths are nondimensionalized with respect to the total cable length L.

B. Extension to Multiple Cables

The equations of motion defined in the last subsection are valid for a single cable. To incorporate an arbitrary number of cables into the simulation requires modifying the boundary conditions at each end of the cable. At the aircraft end, the position of the aircraft is unique for each cable. However, for the payload end, each cable element shares the same payload position for the states corresponding to m_1. To simulate each cable as a standalone object, it is necessary to provide the tension and damping forces from the first cable element of each cable C_j attached to m_1, as shown in Fig. 3. These may be calculated explicitly for each cable object based on the positions and velocities of the payload and first lumped mass representing the cable. Hence, when computing the forces on the end body for cable C_1, the positions and velocities from objects $C_2{:}m_2$ and $C_3{:}m_2$ or the calculated tensions $C_2{:}T_1$ and $C_3{:}T_1$ must be applied to the end body $C_1{:}m_1$. Note that only one cable object needs to maintain the position and velocity of m_1. As will be discussed later, the equations of motion are used to perform numerical linearization around the equilibrium position. For such an application, it is necessary to constrain the position, velocity, and acceleration of the end cable body to be the same for each cable object during the linearization.

Note that the boundary condition at the aircraft is treated as a kinematic constraint. To include the dynamic coupling between an aircraft model and the cable is straightforward, requiring the position of the end of the cable to be replaced by the attachment point of the cable on the aircraft. This coupling is not included in the simulations conducted in this work.

C. Rigid-Body Payload

In the previous subsection, the payload was assumed to be modeled as a point mass. In this section, the extension of the model to consider a rigid-body payload is described. The body axes of the payload are defined with the x_b axis pointing toward the front of the payload, z_b axis down, and the y_b axis completes the right-handed triad. These are the conventional axes used in rigid-body attitude dynamics. We define the Euler angles describing the orientation of the payload relative to the orbital axes. The undisturbed payload x_b axis is aligned with the $\boldsymbol{x}_1$ axis, the y_b axis is aligned with the $-\boldsymbol{x}_2$ axis, and the z_b axis is aligned with the $-\boldsymbol{x}_3$ axis. We use the conventional roll, pitch, and yaw angles to describe the payload orientation, using a 3-2-1 rotation sequence. The direction cosine matrix relating the orbital frame to the payload body frame is given by

$$\mathbf{C}_b^o = \begin{bmatrix} c\theta c\psi & -c\phi s\psi + s\phi s\theta c\psi & s\phi s\psi + c\phi s\theta c\psi \\ -c\theta s\psi & -c\phi c\psi - s\phi s\theta s\psi & s\phi c\psi - c\phi s\theta s\psi \\ s\theta & -s\phi c\theta & -c\phi c\theta \end{bmatrix} \quad (7)$$

where $s(\cdot) = \sin(\cdot)$ and $c(\cdot) = \cos(\cdot)$. The Euler kinematic equations are

$$\dot{\phi} = \omega_x + (\omega_y \sin\phi + \omega_z \cos\phi)\tan\theta$$

$$\dot{\theta} = \omega_y \cos\phi - \omega_z \sin\phi$$

$$\dot{\psi} = (\omega_y \sin\phi + \omega_z \cos\phi)\sec\theta \quad (8)$$

where $\omega = [\omega_x, \omega_y, \omega_z]^T$ is the angular velocity of the payload relative to the orbital axes expressed in the payload body frame,

$$\omega = \omega_I - \omega_O \quad (9)$$

where ω_I is the inertial angular velocity of the payload, and $\omega_O = [\mathbf{C}_b^o]^T[0, 0, \dot{\theta}]^T$ is the angular velocity of the orbital frame expressed in the payload body axes.

The inertial angular velocity is governed by the Euler equations

$$\dot{\omega}_I = \mathbf{I}^{-1}(\mathbf{M}_B - \omega_I \times \mathbf{I}\omega_I) \quad (10)$$

where $\mathbf{I}$ is the inertia matrix. The moments acting on the body are due to aerodynamic loads and tension from the cables. The jth cable is assumed to be attached at a position $\mathbf{p}_j$ from the center of mass, as shown in Fig. 4. The moments due to tension are calculated in the body frame as

$$\mathbf{M}_B^t = \sum_{j=1}^{N_c} \mathbf{p}_j \times (\mathbf{C}_o^b \mathbf{T}_j^{(1)}) \quad (11)$$

where N_c is the number of cables. The aerodynamics of the payload are very important when considering towing in level flight at high speed. For example, certain payload shapes will induce instabilities that may limit the forward speed of the aircraft. However, the aerodynamics are heavily dependent on the shape of the payload and whether or not any active stabilization is provided. Because the aim of this work is to provide a preliminary assessment of the ability to lift large payloads with multiple aircraft, a detailed study of payload aerodynamics is beyond the scope of the paper. In the equilibrium configuration with the aircraft in nominal circular orbits, the payload does not have a linear velocity and hence the contribution of aerodynamic loads is expected to be small. During transition maneuvers or other transient analysis, the aerodynamics become very important.

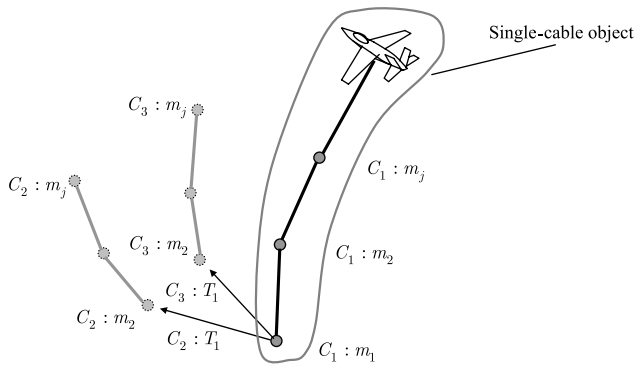

Fig. 3 Modification of cable boundary condition to account for multiple cables.

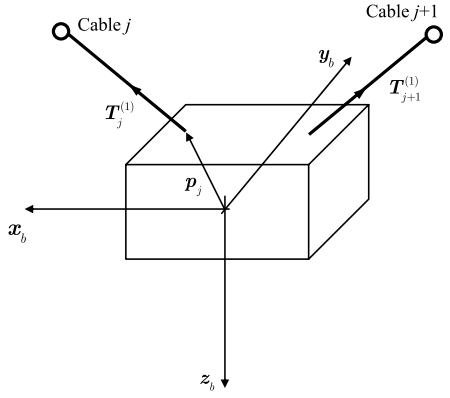

Fig. 4 Geometry of cable attachments on payload.

The method of attaching the cable to the payload is also of significance. In this work, it is assumed that the attachment is performed using a frictionless freely rotating joint. This means that the cable does not twist as the payload rotates. Payload rotation only induces loads due to the offset of the attachment points from the payload center of mass. Simulations taking into account torsion of the lines, and other unsteady payload effects, would be required when considering specific payloads and known attachment configurations. For the purposes of this work, these effects are not considered.

III. Equilibrium Configurations for Multiple-Cable Payload Retrieval

A. Equilibrium Calculations

The determination of cable equilibrium configurations for a multicable system are determined based on relative equilibrium conditions and symmetry. The method used here exploits the fact that the cable system is differentially flat under some mild assumptions [27]. A system is said to be differentially flat if there exists an output, called the flat output, that uniquely determines the system inputs. Differential flatness can be understood by considering a simple undamped oscillator $\ddot{x} + \omega_n^2 x = u$, where x is the coordinate and u is the control input. In this simple case, it is easy to see that x is a flat output, because u may be completely determined by x and its derivatives. This concept extends easily to multidimensional systems involving vectors of inputs and outputs. Essentially, in this work, differential flatness can be viewed as a way of transforming the dynamic system so that the entire motion can be expressed in terms of the flat output and its derivatives. It is easy to show, based on physical principles, that the towed system is differentially flat, with the motion of the towed body as a flat output and the motion of the aircraft as the input. The system is differentially flat if it is assumed that the aerodynamic forces are lumped to each mass only from an adjacent segment, as discussed in Appendix A. We consider the limiting case of relative equilibria, for which the flat output is constant in time when specified in the rotational frame. The position of the payload uniquely determines all forces acting on it except the components of the tension force,

$$\begin{aligned} T_1^{x_1} &= -m_1 q_1 \dot{\theta}^2 - \mathbf{F}_1^a \cdot \mathbf{x}_1 \\ T_1^{x_2} &= -m_1 q_2 \dot{\theta}^2 - \mathbf{F}_1^a \cdot \mathbf{x}_2 \\ T_1^{x_3} &= m_1 g - \mathbf{F}_1^a \cdot \mathbf{x}_3 \end{aligned} \tag{12}$$

However, because of the symmetry of the cable tension forces, it is known that the equilibrium position of the payload is at the origin (assuming equal length cables and the same orbital parameters for the aircraft). Hence, the tension force is primarily in response to the weight of the payload. When the payload is treated as a rigid body, it is assumed that the attachment points of the cables are symmetric around the center of mass, but lie on the upper surface of the payload. Furthermore, to simplify the analysis, the payload is assumed to be axisymmetric. For equilibrium relative to the orbital frame, the payload must have zero pitch and roll angles, and be spinning around the z_b axis at a rate equal to the orbital angular velocity. Because the payload is not translating, it is subjected only to an aerodynamic moment around the z_b axis.

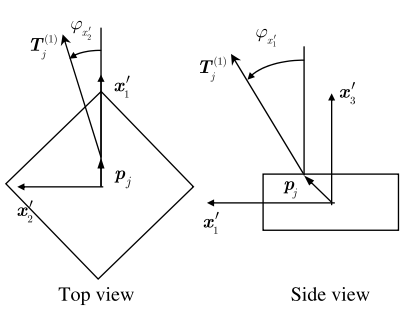

Fig. 5 Orientation of cable at the attachment point on rigid-body payload.

To determine the equilibrium position for a given aircraft orbit, it is necessary to use two iterative parameters, selected here to be the angles of the cable to the vertical, $\varphi_{x_1'}$ and $\varphi_{x_2'}$, as shown in Fig. 5. For convenience, a coordinate frame attached to the center of mass of the payload, but with its x_1' axis aligned with the direction to the tether attachment point in the plane of symmetry is introduced. The tether attachment point using such a definition is given by

$$\mathbf{p} := [p_{x_1'}, 0, p_{x_3'}] \tag{13}$$

For N_c cables, the components of the tension force can be written as

$$\begin{aligned} T_1^{x_1'} &= (m_1 g \tan \varphi_{x_1'})/N_c \\ T_1^{x_2'} &= (m_1 g \tan \varphi_{x_2'})/N_c \\ T_1^{x_3'} &= m_1 g/N_c \end{aligned} \tag{14}$$

Note that it is assumed that all attachment points are located symmetrically on the top surface of the payload. The torque due to the tension is given by

$$\begin{aligned} M_{x_1'} &= p_{x_2'} T_1^{x_3'} - p_{x_3'} T_1^{x_2'} \\ M_{x_2'} &= p_{x_3'} T_1^{x_1'} - p_{x_1'} T_1^{x_3'} \\ M_{x_3'} &= p_{x_1'} T_1^{x_2'} - p_{x_2'} T_1^{x_1'} \end{aligned} \tag{15}$$

In equilibrium, the torque due to tension around the x_3' axis must be balanced by the aerodynamic torque due to yaw rate. If the attachment points are placed symmetrically on the upper surface of the payload, then all torques except $p_{x_1'} T_1^{x_2'}$ sum to zero. During transient motion, all torques influence the payload attitude response and, therefore, they must be taken into consideration. For the case where the payload is treated as a point mass or the aerodynamic torque due to yaw rate is neglected, the tension component $T_1^{x_2'}$ is zero by definition of the $[x_1', x_2', x_3']$ coordinate frame.

For a given unstrained segment length, the tension determines the elongated segment length from Hooke's law,

$$l_1 = L_{s_1}\left(1 + \frac{\sqrt{(T_1^{x_1'})^2 + (T_1^{x_2'})^2 + (T_1^{x_3'})^2}}{EA}\right) \tag{16}$$

and the position of the next mass may be determined as

$$q'_{3(j-1)+i} = \mathbf{p} \cdot \mathbf{x}_i' \delta_{j1} + q'_{3(j-2)+i} + \frac{T_1^{x_i'}}{\sqrt{(T_1^{x_1'})^2 + (T_1^{x_2'})^2 + (T_1^{x_3'})^2}} l_1 \qquad i = 1, 2, 3 \tag{17}$$

where δ_{j1} is the Kronecker delta. The first term accounts for the offset position from the payload center of mass. In general, the tension components in the jth segment may be determined from the equations

$$\begin{aligned} T_j^{x_1'} &= -m_j q'_{3(j-1)+1} \dot{\theta}^2 - F_j^{a_1} + T_{j-1}^{x_1'} \\ T_j^{x_2'} &= -m_j q'_{3(j-1)+2} \dot{\theta}^2 - F_j^{a_2} + T_{j-1}^{x_2'} \qquad j = 2, \ldots, n \\ T_j^{x_3'} &= m_j g - F_j^{a_3} + T_{j-1}^{x_3'} \end{aligned} \tag{18}$$

Following this procedure allows the position of the towpoint to be obtained for prescribed angles $\varphi_{x_1'}$ and $\varphi_{x_2'}$. For the case when the aircraft orbit radius is fixed, an iterative process is required until the end of the cable matches the orbit radius of the aircraft. The accuracy of the cable shape increases as the number of segments representing the cable increases. Once the procedure converges, the cable and aircraft positions are transformed into any desired relative configuration based on the number of cables using the rotation angle

Table 1 Nominal cable and aircraft parameters

Property	Value
Cable density	970 kg/m^3
Modulus of elasticity	120 GPa
Cable diameter	10 mm
Ultimate tensile strength	450 GPa
Damping constant	5000 N · s
Aircraft mass	30,000 kg
Wing area	120.77 m^2
Wing span	30.37 m
Lift curve slope	4.68/rad
Parasitic drag coefficient	0.015
Lift-induced drag coefficient	0.0617

$$\Theta_j = \Theta_0 + 2\pi\frac{(j-1)}{N_c} \tag{19}$$

where Θ_0 is the arbitrary angle of the first aircraft to the x_1 axis. After transforming the solution via the angle Θ_j, the cable coordinates in the nominal orbital axes are obtained.

The required aircraft performance parameters may be determined using some simple aerodynamic data for a given aircraft and considering the equilibrium requirements for the aircraft (see Appendix B). The key limitations of the aircraft for the single-cable circularly towed system are stall limit, bank limits, thrust/power limits, and load factor. The performance limitations are calculated taking into account the effect of the steady-state cable tension.

B. Payload Pickup

One of the best features of a multicable payload pickup system is that there are a wide range of combinations of system parameters that can be selected without influencing the equilibrium position of the payload. That is, the payload is always balanced at the origin due to symmetry. Thus, it is possible to use a much larger range of aircraft types without being overly concerned with the aircraft's ability to turn extremely tight circles as is required in the case of a single cable. This also allows the cable to be designed to withstand the tensile loads without the drawback of the adverse effects of an increase in weight.

In this section, we have selected the Orion PC-3 aircraft as the nominal aircraft type. In this work, some rough parameters for this aircraft are used, as taken from [17]. The Orion PC-3 is used by the Australian military and would be suitable for picking up relatively large payloads. The nominal system parameters are given in Table 1 for a spectra tether. Throughout this section, a two-cable configuration is considered for the analysis as this simplifies the complexity of a practical implementation of the technique.

1. *1500 Meter Cable*

Figure 6 shows numerical results for the required aircraft bank angle and lift coefficient generated with each cable discretized into 100 segments and an aircraft speed of 70 m/s. Lines of constant payload mass between 500 and 10,000 kg are shown as a function of the aircraft orbit radius. Figure 6 shows, as expected, that an increase in payload mass leads to an increase in the required lift coefficient. However, it also reveals that the change per 500 kg is not particularly significant. An increase in orbit radius leads to a much larger decrease in the required lift coefficient except as the radius approaches the cable length. Interestingly, an increase in payload mass leads to a decrease in the required bank angle. In fact, as the orbit radius approaches the cable length, the bank angle reverses sign for large payloads. This occurs because of the large component of cable tension directed toward the center of the circle. Figure 6 also shows that there is a very large range of orbit radii for which it is possible to pick up very large payloads. It is clear that the two-cable system is far superior to a single-cable system, which has a very narrow range of orbit radii and small payload masses [17].

Figures 7 and 8 show examples of the cable shapes produced by the maneuver for various orbit radii for 500 and 5000 kg payloads, respectively. In all cases, the cable takes on a full three-dimensional shape due to the effects of aerodynamic drag. The cable profile is projected onto the walls of the plots in Figs. 7 and 8. These plots show that increasing the payload mass for a given orbit radius tends to straighten the cable, whereas increasing the aircraft orbit radius (approaching the cable length) leads to a decrease in the required aircraft altitude and bank angle. This has implications for the design of aerial maneuvers using such a system. For example, if the aircraft altitude is fixed, a simultaneous increase in orbit radii of the aircraft would lead to an increase in the altitude of the payload, that is, lifting the payload.

2. *3000 Meter Cable*

Figure 9 shows the required aircraft bank angle and lift coefficient for lifting various size payloads with a 3-km-long cable. Figures 10 and 11 show the equilibrium cable shapes for a 500 kg payload and a

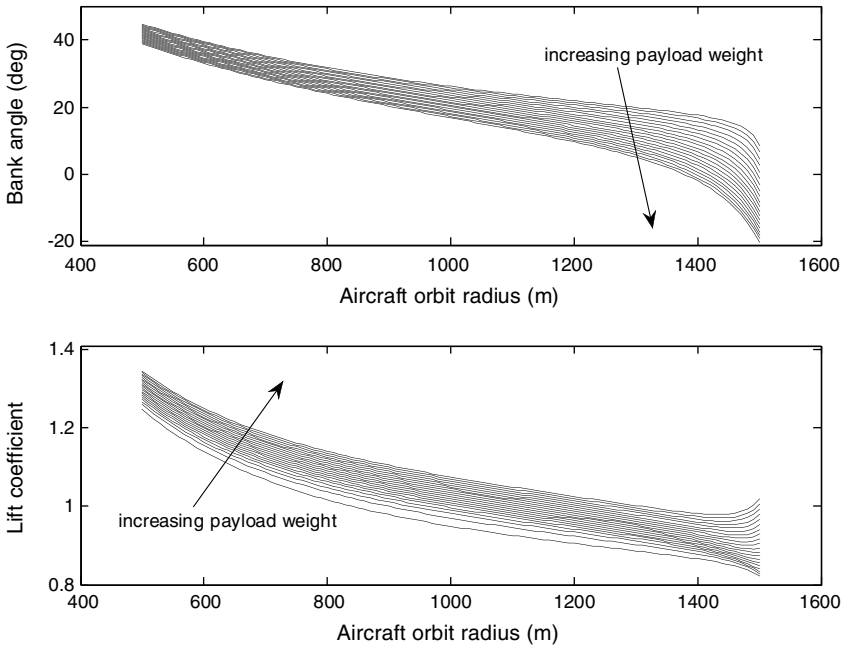

Fig. 6 Effect of payload mass and orbit radius on required aircraft bank angle and lift coefficient for 1500 m cable, lines of constant payload mass from 500–10,000 kg at 500 kg intervals.

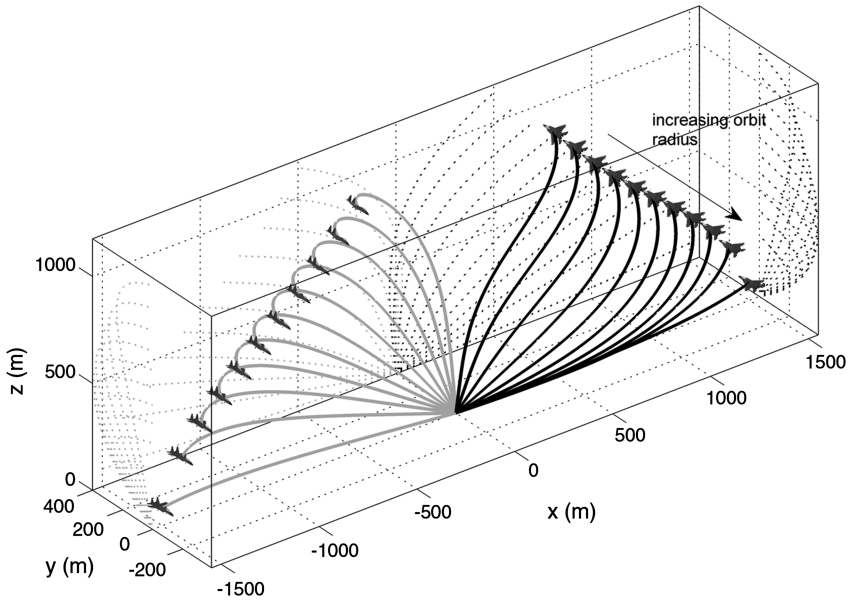

Fig. 7 Equilibrium cable shapes for a 500 kg payload with a cable length of 1500 m, $V = 70$ m/s. Projections of cable shape shown on walls of plot.

5000 kg payload, respectively, for various aircraft radii. The increase in cable length relative to the 1.5 km cable leads to higher requirements for the aircraft lift coefficient due to the doubling of the cable mass as well as the increase in cable drag. Comparing Figs. 10 and 11 also illustrates the significant effect that the payload mass has on the cable shape. A larger payload mass leads to a straighter cable while in the equilibrium position, due to the increased cable tension. The results also suggest that the aircraft orbit radius should be large rather than small, as it results in smaller required bank angles and lift coefficients. This ensures that the aircraft performance parameters are well within the aircraft limits, as well as keeping the aircraft at a relatively low altitude where observation of the payload can be achieved by the pilot(s).

Figure 12 shows the effect of varying the aircraft speed for a constant orbit radius of 1000 m. Figure 12 shows that the aircraft lift coefficient is more sensitive to speed than orbit radius. For a 1 km orbit radius, speeds greater than about 70 m/s result in realistic lift coefficients (<1.1) and bank angles. It can also be seen that increases in speed lead to higher bank angles, due to the need to maintain larger lateral accelerations. Figure 13 shows the equilibrium cable shapes for a 500 kg payload for various aircraft speeds. Figure 13 shows that, for a 500 kg payload, increasing the aircraft speed decreases the required aircraft altitude. This is due to the larger drag on the cable, which gives it a larger component of tension in the horizontal plane.

C. Modal Analysis

In this section, a linear modal analysis is performed for a two-aircraft system with a 5000 kg payload, aircraft speed of 70 m/s, orbit radius of 700 m, and a 3-km-long cable. The drag parameter of the payload is assumed to be $C_D A = 5$ m^2. The cable discretization is 100 elements for each cable. The linear stability and modal analysis is carried out by using a central finite difference approximation around the equilibrium configuration to determine the system Jacobian. The corresponding eigenvalues and eigenvectors of the Jacobian reveal the modal and stability properties of the particular

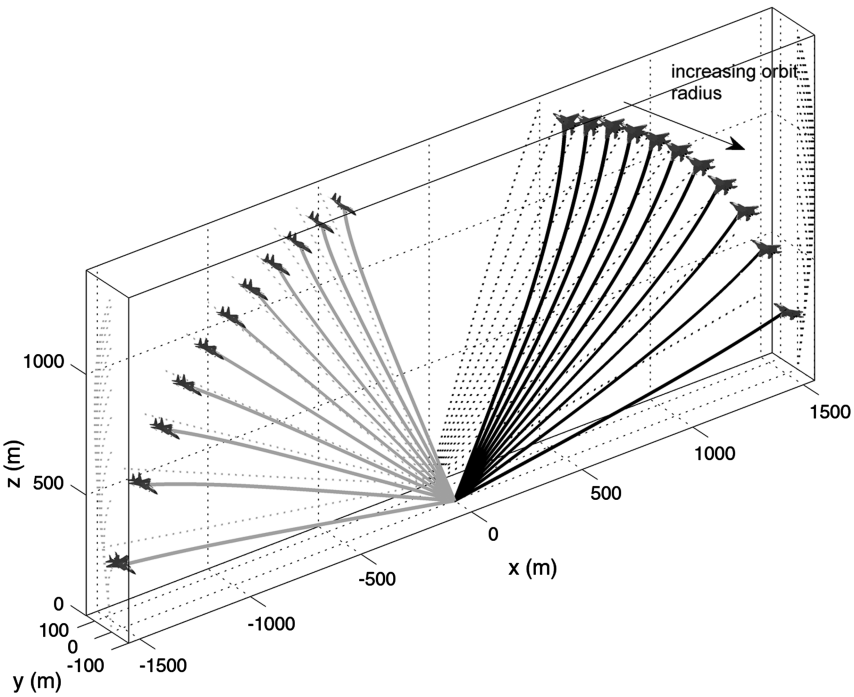

Fig. 8 Equilibrium cable shapes for a 5000 kg payload with a cable length of 1500 m, $V = 70$ m/s. Projections of cable shape shown on walls of plot.

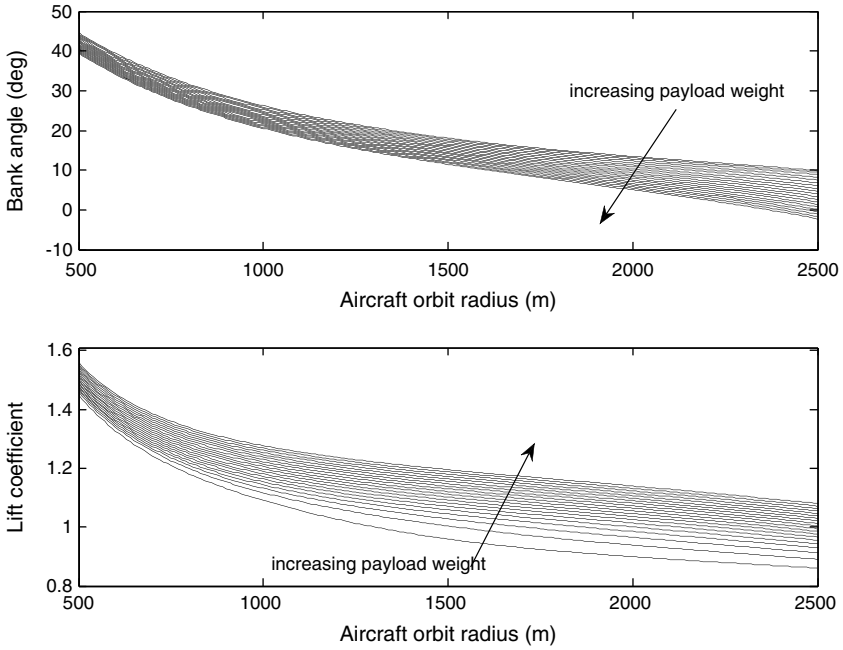

Fig. 9 Effect of payload mass and orbit radius on required aircraft bank angle and lift coefficient for 3000 m cable, lines of constant payload mass from 500–10,000 kg at 500 kg intervals.

configuration. Figure 14 shows the first six mode shapes and natural frequencies of the system. The first-mode is a rigid-body-type motion of the payload, which results in the payload spiraling in the direction of the orbit when viewed in the inertial frame. The second mode resembles a fundamental string mode for each cable, which couples to heaving of the payload in the vertical plane. This is due to this mode being symmetric. The third mode is a spiraling type motion of the payload when viewed in the rotating frame, but the direction of the payload opposes the orbital motion of the system. This mode is lightly damped compared to the first two modes (damping ratio 0.2 compared with 0.64 and 0.72 for the first two modes). The third mode resembles the third mode of the single-cable towed system (see Fig. 9c in [17]) The fourth mode is a highly damped coupled string and lateral translation mode of the payload. This is an asymmetric mode. The fifth mode is the second string mode of each cable and is symmetric about the vertical plane. The sixth mode is a symmetric higher-order string mode that couples with heaving of the payload. The modal analysis shows that the fundamental modes are stable and have relatively high damping ratios. This result is superior to that of a single-cable system, where the fundamental modes have comparatively low damping ratios [minimum 0.07 damping ratio (Figs. 7 and 8 in [17]) compared with a minimum of 0.2 for the current configuration]. The difference in minimum damping ratio is largely due to the restoring force of the second cable acting on the payload, whereas a single-cable system has to rely on aerodynamic damping alone.

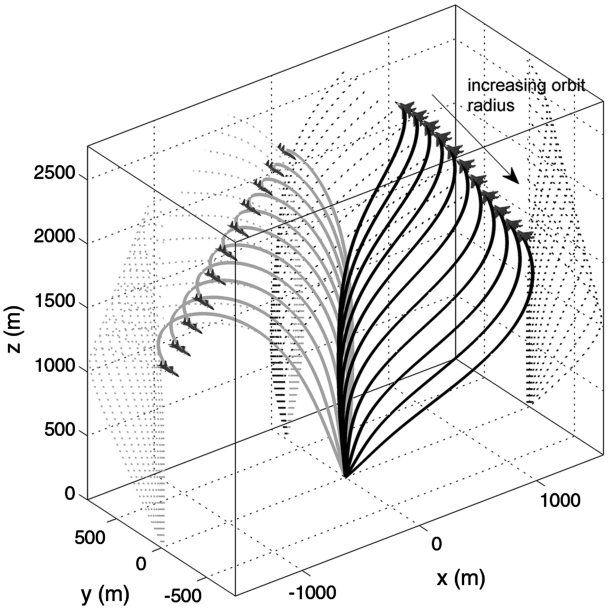

Fig. 10 Equilibrium cable shapes for a 500 kg payload with a cable length of 3000 m, $V = 70$ m/s. Projections of cable shape shown on walls of plot.

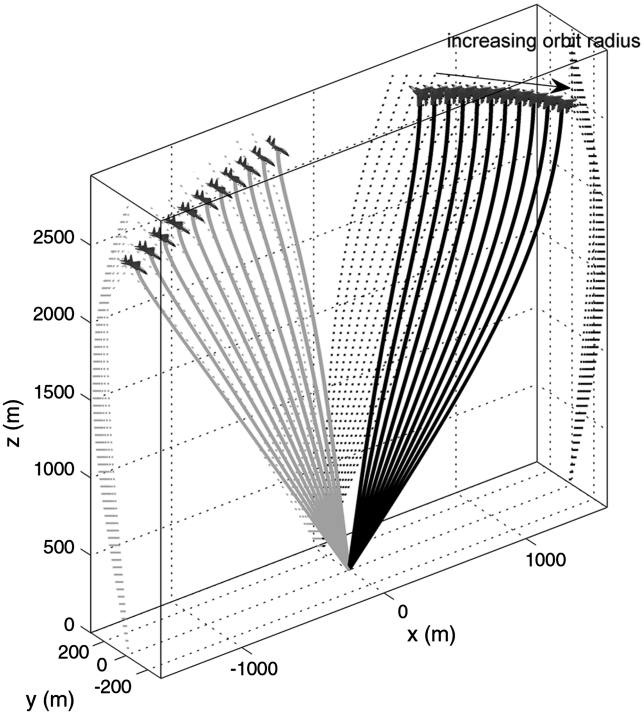

Fig. 11 Equilibrium cable shapes for a 5000 kg payload with a cable length of 3000 m, $V = 70$ m/s. Projections of cable shape shown on walls of plot.

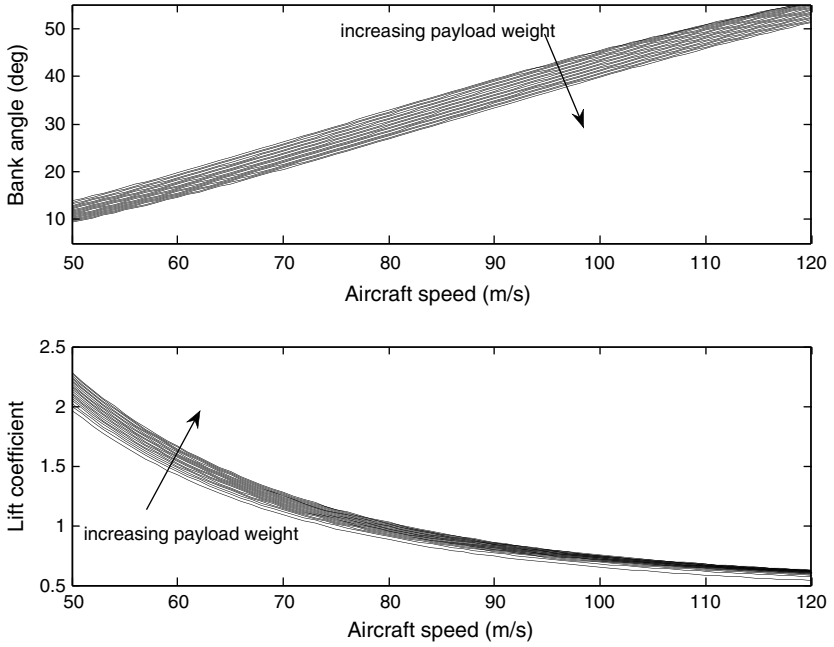

Fig. 12 Effect of payload mass and aircraft speed on required aircraft bank angle and lift coefficient for 3000 m cable, lines of constant payload mass from 500–10,000 kg at 1000 kg intervals and $R = 1000$ m.

IV. Transition Maneuver Design

Transitioning from circular flight to straight and level flight must be timed carefully to avoid cable tangling or collision of aircraft. The maneuver design phase must also take into account bank angle limits, thrust limits, and stall limits of the aircraft. To make the maneuver design as general as possible, the trajectory is shaped in the rotating frame rather than the inertial frame. This ensures, for example, that two aircraft will always move relative to each other in the design space. It also reduces the complexity of the trajectory and allows the use of low-order polynomials for shaping the path.

The basic principle of the transition is to find a polar coordinate map for each aircraft such that the initial speed is the speed of the circular orbit, and the final aircraft speed is the desired level flight speed. If the trajectory of the aircraft in the rotating frame is expanded as power series with time as the independent variable we have

$$R = a_R^0 + a_R^1(t-t_0) + a_R^2(t-t_0)^2 + \cdots + a_R^n(t-t_0)^n$$
$$\chi = a_\chi^0 + a_\chi^1(t-t_0) + a_\chi^2(t-t_0)^2 + \cdots + a_\chi^n(t-t_0)^n \qquad (20)$$

where t_0 is the maneuver start time. Figure 15 shows the definition of the radius and polar angle used in the trajectory definition.

The initial position of the aircraft in the rotating frame is dependent on the particular aircraft in question. For the baseline case considered in this paper, we have $\chi_0 = \Theta_j$ for aircraft j. The final angular position of the jth aircraft must be equal to the angular position of all other aircraft. For simplicity, we define the aircraft on the x_1 axis as the leader and refer the motion of all other aircraft to it. Hence, the final angle of all aircraft is given by $\chi_f = 0$.

Assume that the nominal aircraft orbit radius is R_0, and the orbital speed is V_0. During the transition, the orbit radius increases to R_f, with an associated increase in speed to V_f. For the transition to be smooth, the following constraints should be enforced:

$$\dot{R}_0 = \dot{R}_f = \ddot{R}_0 = \ddot{R}_f = \ddot{\chi}_0 = \ddot{\chi}_f = 0 \qquad (21)$$

To match the desired speeds, we have that

$$\dot{\chi}_0 = V_0/R_0 - \dot{\theta} \qquad (22)$$

$$\dot{\chi}_f = V_f/R_f - \dot{\theta} \qquad (23)$$

By selecting fifth-order polynomials, all coefficients can be solved uniquely as a function of the maneuver time $t_m \triangleq t_f - t_0$, which acts as a tuning parameter. Using these relationships, we have the following definition of the transition maneuver:

$$R = R_0 + 10\frac{(R_f - R_0)}{t_m^3}(t-t_0)^3 + 15\frac{(R_0 - R_f)}{t_m^4}(t-t_0)^4 + 6\frac{(R_f - R_0)}{t_m^5}(t-t_0)^5 \qquad (24)$$

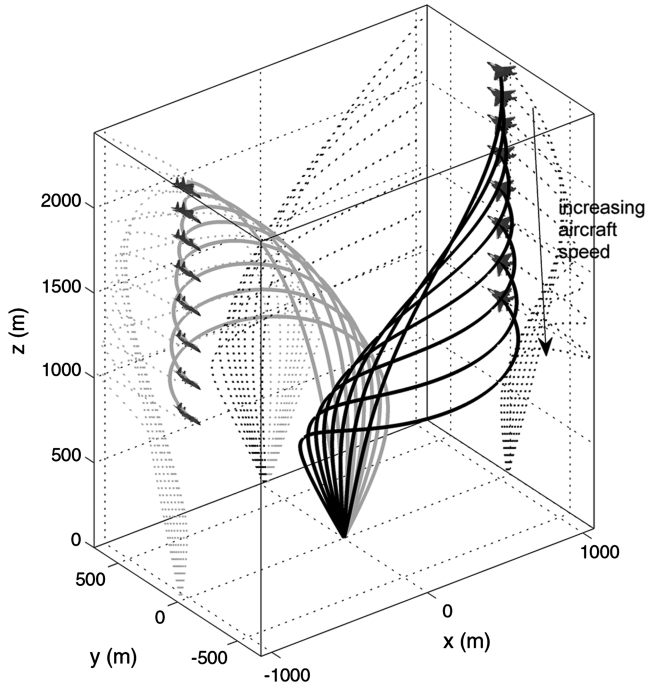

Fig. 13 Equilibrium cable shapes for a 500 kg payload for different aircraft speeds with a cable length of 3000 m, $R = 1000$ m (50–120 m/s). Projections of cable shape shown on walls of plot.

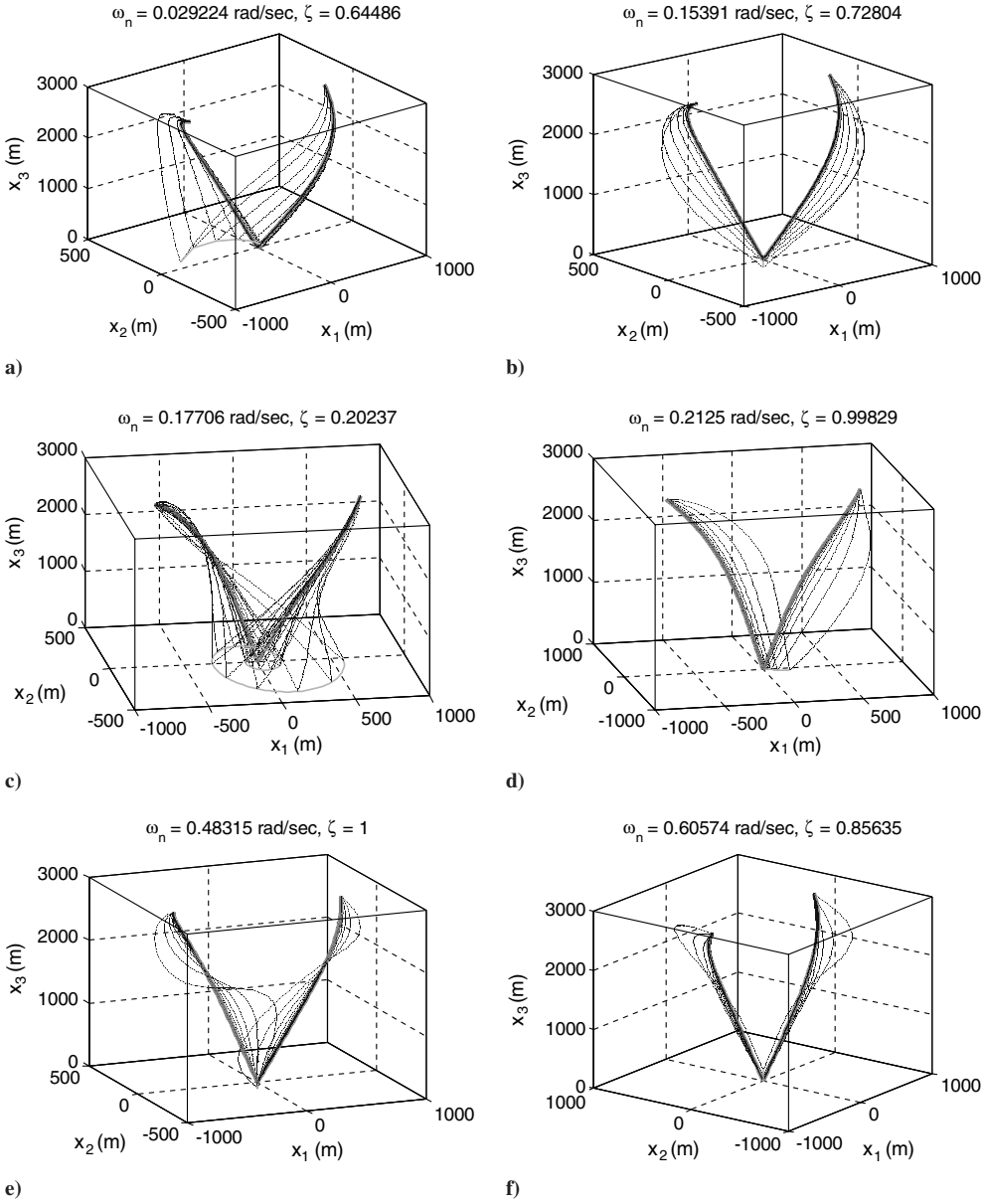

Fig. 14 Mode shapes of system for 5000 kg payload, 3000-m-long cable, $R = 700$ m, $V = 70$ m/s, and $C_DA = 5$ m^2: a) mode 1, b) mode 2, c) mode 3, d) mode 4, e) mode 5, and f) mode 6.

$$\chi = \chi_0 + \left(\frac{v_0}{R_0} - \dot{\theta}\right)(t - t_0) + \left[10\frac{(\chi_f - \chi_0)}{t_m^3} - \frac{6}{t_m^2}\left(\frac{v_0}{R_0} - \dot{\theta}\right) - \frac{4}{t_m^2}\left(\frac{v_f}{R_f} - \dot{\theta}\right)\right](t - t_0)^3 + \left[15\frac{(\chi_0 - \chi_f)}{t_m^4} + \frac{8}{t_m^3}\left(\frac{v_0}{R_0} - \dot{\theta}\right) + \frac{7}{t_m^3}\left(\frac{v_f}{R_f} - \dot{\theta}\right)\right](t - t_0)^4 + \left[6\frac{(\chi_f - \chi_0)}{t_m^5} - \frac{3}{t_m^4}\left(\frac{v_0}{R_0} - \dot{\theta}\right) - \frac{3}{t_m^4}\left(\frac{v_f}{R_f} - \dot{\theta}\right)\right](t - t_0)^5 \tag{25}$$

Using these expressions, and neglecting the influence of the cable, the thrust, lift coefficient, and bank angle can be calculated as a function of time during the proposed maneuver. The maneuver time is adjusted until the variation in speed, lift coefficient, and bank angle are realistic. Once a maneuver has been designed, it is simulated using the full nonlinear equations of motion for the system. This provides a time history of cable loads on the aircraft. Using these loads, the aircraft thrust, lift coefficient, and bank angle time histories are recomputed. Hence, the resulting aircraft performance parameters include the effect of the cable, which tend to have a large effect for heavy loads. In practice, the presence of large cable tension is a significant disturbance to the aircraft and must be accounted for in the flight control system. Measurements of the tension force and direction in the aircraft body frame would be required to design a tension compensator for the aircraft autopilot. Hence, turbulence, payload rotations, and navigation errors that create transients in the tension force could be mitigated to a degree by the autopilot. A full closed-loop simulation with a model of the flight control laws is the subject of future work.

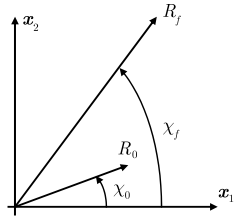

Fig. 15 Geometry of initial and final aircraft orbit positions in rotating frame.

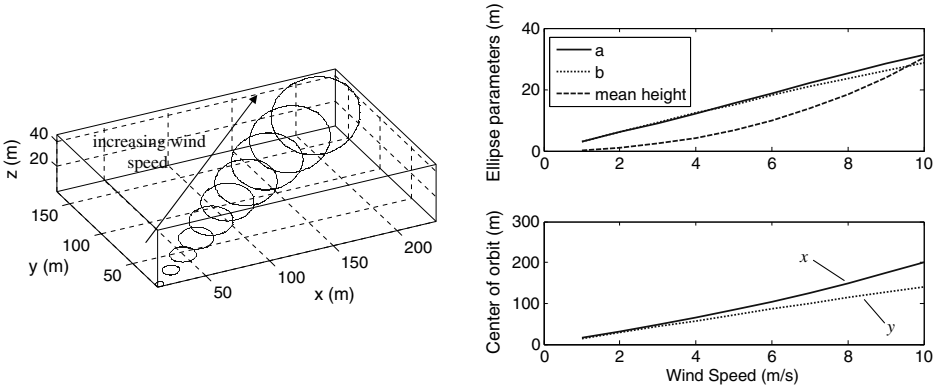

a) b)

Fig. 16 Effect of wind on payload orbit: a) trajectories in inertial coordinates, and b) derived payload orbit parameters (semimajor axis a, semiminor axis b).

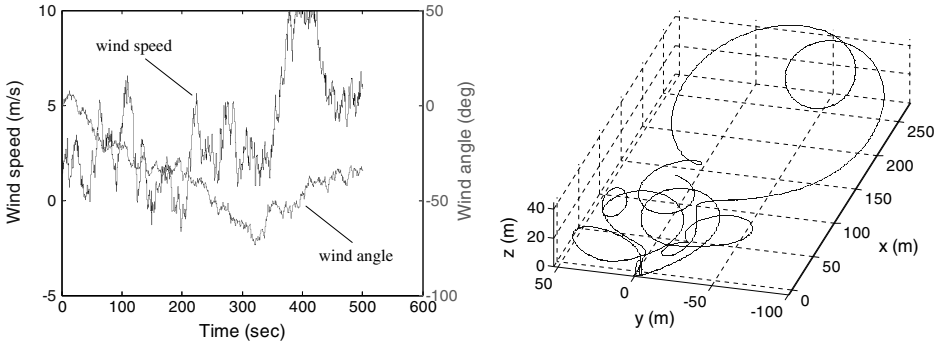

a) b)

Fig. 17 Effect of random winds on payload trajectory: a) wind speed and direction, and b) trajectory of payload in inertial coordinates.

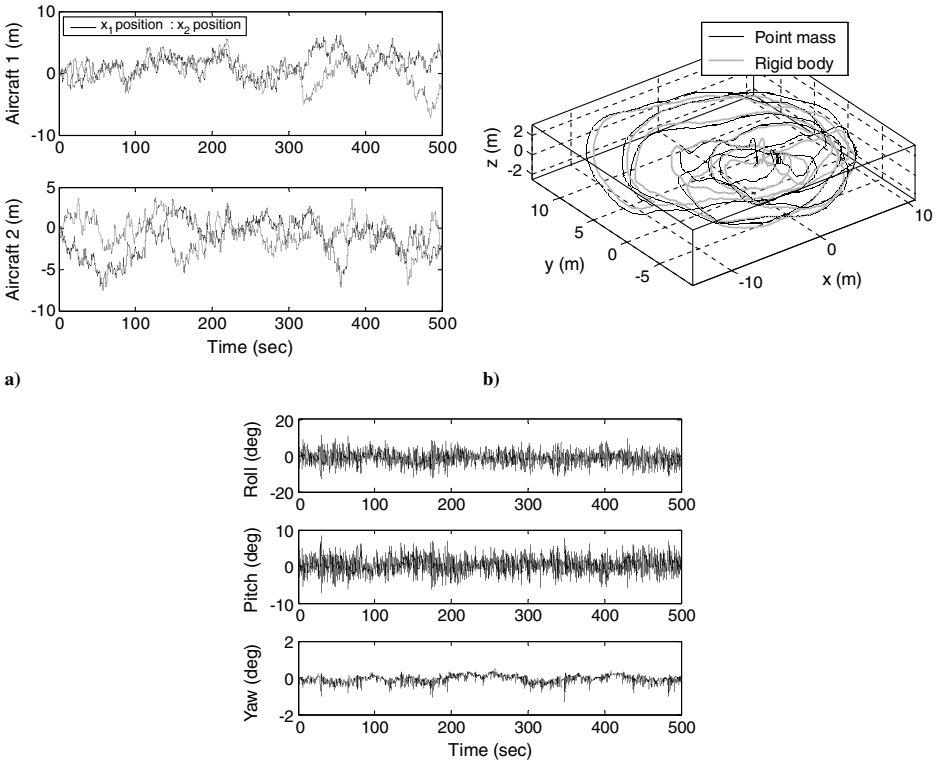

a) b) c)

Fig. 18 Effect of aircraft disturbances on payload response: a) aircraft position errors in rotating frame (x_1 position, x_2 position), b) payload response in inertial frame, and c) attitude response of rigid-body payload.

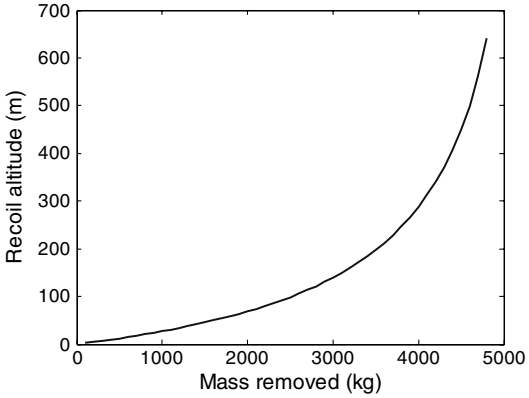

Fig. 19 Recoil of payload due to mass removal.

V. Numerical Results

A. Transient Behavior

In this section, the transient dynamics of the system due to the following effects are presented: 1) crosswinds, 2) disturbances in aircraft position, and 3) removal of mass from payload. Each of these effects are simulated using the same baseline system that was used for the modal analysis. In all cases, the nonlinear equations of motion are integrated starting from the relative equilibrium configuration. A point mass payload is assumed unless otherwise stated.

1. Effect of Crosswinds

The effect of crosswinds is first assessed by simulating winds with constant speed and direction. The effect of wind strength is shown in Fig. 16a, which shows the trajectory of the payload in inertial coordinates due to a constant wind in the direction of the inertial x axis. The payload is initially at the origin, and only the steady-state orbit is shown. As expected, the payload orbit drifts downwind, with the disturbance size growing with wind speed. In general, a steady-state offset can be easily compensated for by shifting the center of the aircraft orbit, whereas the induced dynamic motion is harder to control. The results show that the wind does not induce a pure downwind offset. Instead, there is an induced offset to the payload orbit in a direction that coincides with the orbital motion. Figure 16b shows the derived orbital parameters of the payload due to the effect of wind. It shows that, for low wind speeds, the shift in payload orbit is roughly equal in the down- and crosswind directions. However, as the wind speed increases, the shift downwind is larger than the crosswind drift. Because the cable lengths are fixed, the horizontal movement of the payload orbit results in an increase in the mean payload altitude. The payload orbit is circular for low wind speeds, but becomes slightly elliptical as the wind speed increases. Figure 16b shows the ellipse parameters (semimajor axis a and semiminor axis b) as a function of the wind speed. The results show that the dynamic motion of the payload for a 6 m/s wind speed is a circle with a radius on the order of 20 m. The induced steady-state velocity of the payload is approximately 2 m/s.

Figure 17 shows the results of a simulation with wind speed and direction governed by a white-noise-driven random walk process. The results show that the motion of the payload is driven mostly in the first mode of the system, with varying amplitude depending on the wind strength. The results for an unsteady wind match the derived steady-state behavior shown in Fig. 16 quite well. For example, when the wind speed is less than 5 m/s, the motion of the payload is bounded to a region with a radius of approximately 50 m. When the wind speed peaks at 10 m/s, the payload is pushed away from the center of orbit by approximately 200 m. The specific system under consideration here is best suited to wind speeds less than approximately 5 m/s. For higher wind speeds, the unsteady motion makes precision targeting more difficult. For some applications, anchoring the payload in high-wind conditions may be necessary [21].

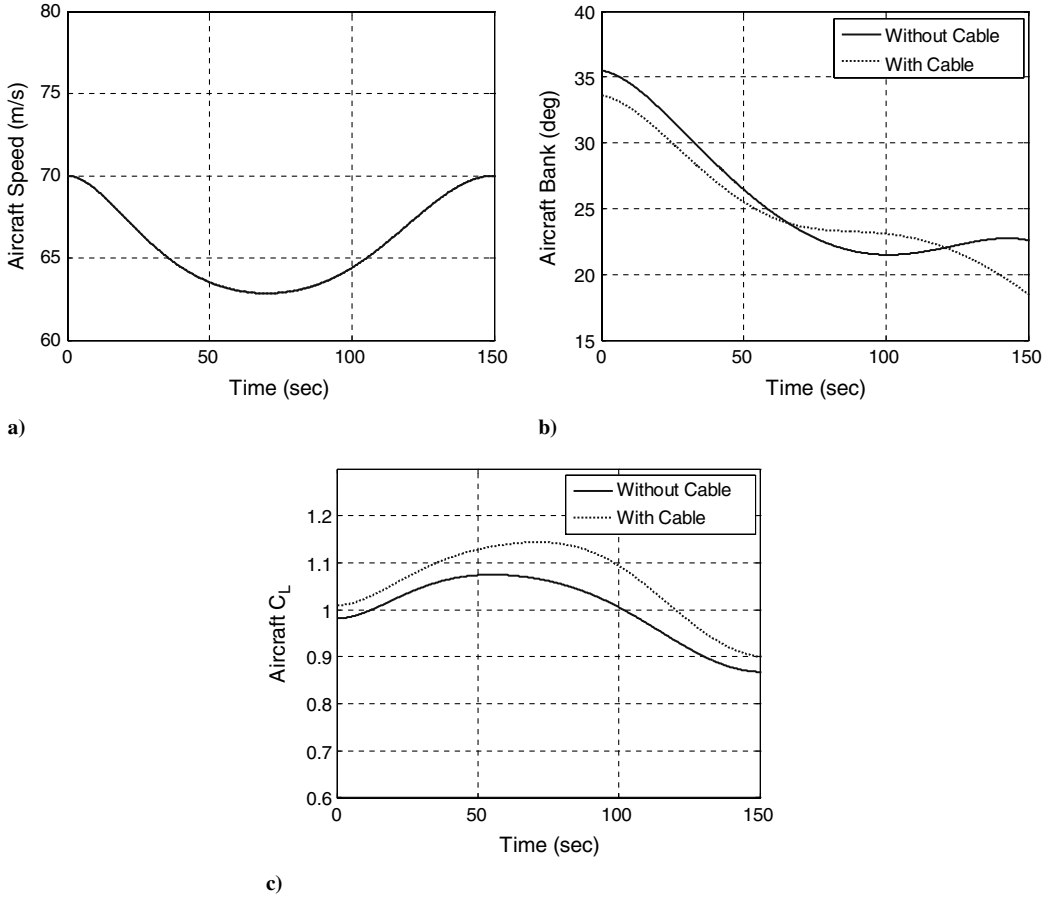

Fig. 20 Approximate aircraft performance requirements for second aircraft in three aircraft transition maneuver.

2. Effect of Aircraft Disturbances

Aside from wind disturbances, a practical system will also be subjected to errors in aircraft positioning due to navigation errors as well as tracking errors. Figure 18 shows simulation results of the effect of random walk errors in the position of the aircraft in the rotating frame. Errors in position also translate to velocity errors in the inertial frame. The payload response is shown in Fig. 18b, which shows that the magnitude of the error in payload positioning is roughly equal to the sum of the errors in the two aircraft positions. The payload dynamic response is largely a spiraling motion, corresponding to the first and third modes of the system. Figure 18b also shows simulation results with the payload modeled as a rigid body with inertias $I_x = I_y = I_z = 1000$ kg $\cdot$ m^2, and with the attachment points located at $\mathbf{p}_1 = [5, 0, 1]$, $\mathbf{p}_2 = [-5, 0, 1]$ m in the payload body axes. In this case, the difference between a point mass and rigid-body payload is relatively small. Figure 18c shows the time history of the payload Euler angles, which show that the disturbances in aircraft positioning lead to pitch and roll motions of less than 10 deg. In comparison, the yaw angle error is considerably smaller (less than 1.5 deg). This is because the out-of-plane disturbances to the tension at the payload end are significantly smaller for this case than the in-plane tension oscillations, that is, the angle $\varphi_{x_2'}$ in Fig. 5 is small. The majority of the positioning error of the payload is on the order of 5 m. This is roughly on the same order of magnitude of a nondifferential Global Positioning System that could be used for targeting.

3. Effect of Mass Removal

If a payload is to be delivered using such a system without anchoring the cable, it is inevitable that the tension stored in the tethers will cause the payload to recoil when mass is removed. Simulations were performed with the sudden removal of mass from the payload. The initial payload mass is 5000 kg, and the mass removed was varied from 100 to 4800 kg. Figure 19 shows the maximum recoil altitude of the remaining mass. As expected, the change in altitude of the mass remaining is strongly dependent on the amount of mass removed. For small mass removal, the change in altitude is on the order of a few meters. However, for significant changes in mass, the recoil can be up to 600 m. Because of symmetry in the system, the payload response is primarily in the vertical plane. However, this assumes the payload is at the center of the circle at the time of mass removal. If the payload is not in equilibrium at the instant of mass removal, it will respond with a combination of spiraling and flexible modes. These results show the need for relaxing the cable tension before removal of mass. This could be achieved, for example, by mounting the payload on the ground and reducing aircraft altitude or by reeling the cables out once the payload

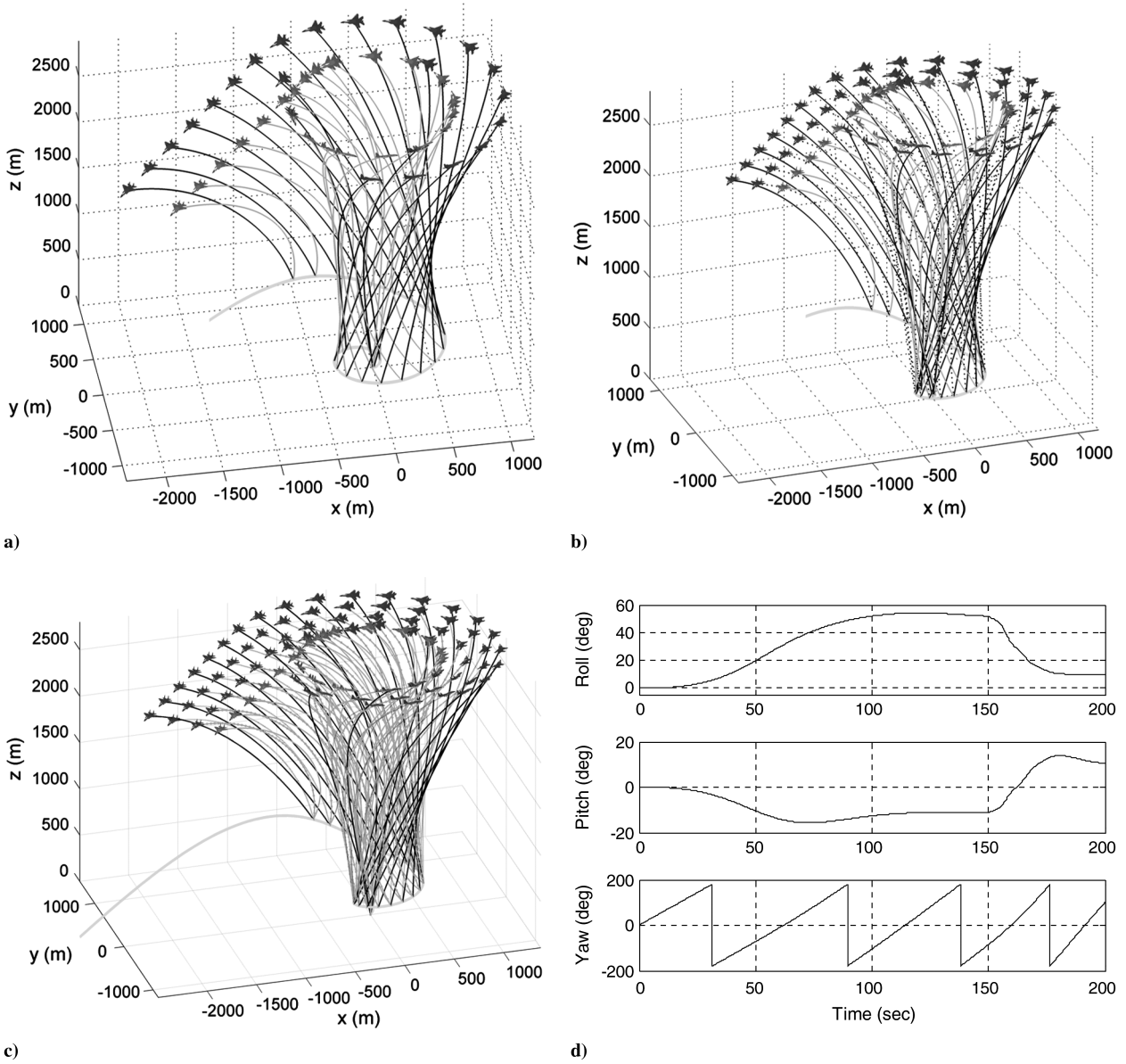

Fig. 21 Multiple-aircraft payload lifting maneuver: a) two aircraft, b) three aircraft, c) four aircraft, d) inertial-to-body Euler angles of payload for two-aircraft maneuver.

is in contact with the ground. The reduction in tension would prevent the large vertical oscillations of the payload shown in Fig. 19.

B. Transition from Circular to Straight Flight

In this section, the transition maneuver described in Sec. IV is simulated using the nonlinear dynamic equations of the cable system. Separate simulations are carried out for systems comprising two, three, and four aircraft/cables. The system parameters remain the same as those used for the modal analysis. The maneuver is designed with a transition time of 150 s, and the final aircraft speed is chosen to be equal to the initial orbital speed of 70 m/s. A maneuver time of 150 s was found to give a good balance between a fast maneuver time and smooth transition dynamics for the aircraft. The maneuver is designed to maintain the leader aircraft in the nominal circular orbit until the follower aircraft complete the transition. The second aircraft complete(s) the maneuver with a radius increase of 250 m. For the case of a three-aircraft maneuver, the second aircraft increases its radius by 250 m and the third aircraft increases its orbit radius by 500 m. For the case of a four-aircraft maneuver, the second aircraft increases its radius by 250 m, the third aircraft increases its orbit radius by 500 m, and the fourth aircraft increases its orbit radius by 750 m. The maneuver design ensures that no two aircraft collide.

The approximate calculations used for analyzing the maneuver are shown in Fig. 20 for the second aircraft. Figure 20 shows the design results without the effect of cable tension, and the revised calculations with the effects of cable tension following a dynamic simulation of the cable response. Figure 20a shows that the aircraft speed decreases by approximately 7 m/s before increasing to the nominal speed of 70 m/s. Figure 20b shows the aircraft bank angle, and Fig. 20c shows the variation in lift coefficient. The results illustrate the importance of accounting for the tension of the cable in the aircraft performance calculations, that is, there is an approximate 10% increase in the peak lift coefficient for this maneuver.

Figure 21 shows time-lapse plots of the aircraft motion and cable responses during the maneuvers with two, three, and four aircraft, respectively. The trajectory of the payload is very similar in all three maneuvers. The cable dynamics are very smooth, and a steady-state equilibrium is achieved relative to the towing aircraft quickly, without residual oscillations of the cable/payload. These results illustrate the effectiveness of the transition maneuver design. Figure 21d shows the rigid-body response of the payload for the two-aircraft transition maneuver. The payload parameters are the same as those used in Sec. V.A.2. Note that the yaw angle shown in Fig. 21d is from body to inertial, rather than from body to orbital. This plot shows that the payload pitches down (15 deg) and rolls to its right (50 deg) during the transition. This is due solely to the variation in tension force on the cables, and does not take into account any aerodynamic effects. The disturbances to the payload attitude can therefore be significant and need to be modeled accurately before implementing the technique in practice. Other systematic errors will likely cause additional payload rotations and oscillations, and Monte Carlo simulations should be conducted before flight implementation of the transition maneuver.

VI. Conclusions

The dynamics of a multicable–multi-aircraft system for retrieving payloads has been studied using numerical simulations. The specific case of a twin-cable system has been studied in detail, and has been found to be far superior to a single-cable system. The most significant advantage is that the two-cable system allows virtually any combination of aircraft operating parameters to be used, whereas, in the case of a single cable, the aircraft must fly very close to its performance limits. The difference is due to the symmetric cable tension forces acting on the payload, which cause the payload to remain at the center of the circle in the equilibrium configuration, regardless of the aircraft orbit. A modal analysis demonstrates the stability of the system as well as the predominant cable modes influencing the system dynamics. The fundamental modes are well-damped compared to the fundamental modes of a single-cable system, which allows better dynamic positioning of the payload in the presence of wind and aircraft disturbances. Transition to forward flight can be achieved by planning the trajectories of any number of aircraft relative to a leader aircraft. By timing the maneuver appropriately, all aircraft cross at the same position, where forward flight is initiated. Simulations show that this procedure is very smooth, with little oscillation of the payload position. The attitude of the payload undergoes large pitch and roll motions during the transition, and should be accounted for. Unsteady aerodynamic effects of the cables and payload in forward flight are also very important, and their effects need to be assessed through detailed simulations.

Appendix A: Lumped Mass Cable Force Models

The force models for each cable object are outlined in this Appendix for completeness.

I. Elastic Tension Forces

Consider the strain in the jth cable segment,

$$\varepsilon_j = \begin{cases} \frac{|\mathbf{l}_j| - L_{s_j}}{L_{s_j}}, & |\mathbf{l}_j| \geq L_{s_j} \\ 0, & |\mathbf{l}_j| < L_{s_j} \end{cases} \tag{A1}$$

where $\mathbf{l}_j$ is the displacement vector of the jth mass relative to the $(j+1)$th mass

$$\mathbf{l}_j = \sum_{i=1}^{3} (q_{3(j-1)+i} - q_{3j+i})\mathbf{x}_i \tag{A2}$$

The tension force can then be defined according to Hooke's law as

$$T_j = EA\varepsilon_j \tag{A3}$$

where E is the Young's modulus of the cable, and A is the cross-sectional area. The total force due to tension on the jth mass is given by

$$\mathbf{F}_j^s = T_{j-1}\frac{\mathbf{l}_{j-1}}{|\mathbf{l}_{j-1}|} - T_j\frac{\mathbf{l}_j}{|\mathbf{l}_j|} \tag{A4}$$

II. Damping Forces

The damping forces in the cable are assumed to be proportional to the strain rate. The length of the jth segment may be expressed as

$$l_j = L_{s_j}(1 + \varepsilon_j) \tag{A5}$$

Taking the time derivative of Eq. (A5) and rearranging

$$\dot{\varepsilon}_j = \frac{\dot{l}_j}{L_{s_j}} - \frac{\dot{L}_{s_j}}{L_{s_j}}(1 + \varepsilon_j) \tag{A6}$$

with

$$\dot{l}_j = \dot{\mathbf{l}}_j \cdot \frac{\mathbf{l}_j}{|\mathbf{l}_j|} \tag{A7}$$

The damping force in the jth segment is given by

$$D_j = \begin{cases} C\dot{\varepsilon}_j, & \varepsilon_j \geq 0 \\ 0, & \varepsilon_j < 0 \end{cases} \tag{A8}$$

The total force due to damping on the jth mass is

$$\mathbf{F}_j^d = D_{j-1}\frac{\mathbf{l}_{j-1}}{|\mathbf{l}_{j-1}|} - D_j\frac{\mathbf{l}_j}{|\mathbf{l}_j|} \tag{A9}$$

III. Aerodynamic Drag Forces

The aerodynamic forces on the cable are modeled by decomposing the flow into components normal and tangential to the cable. Any components of the forces due to effects such as vortex shedding or

unsteady flow are not treated in the model. Consider the geometry of the cable system shown in Fig. A1.

The aerodynamic forces on the jth mass are calculated using the relative velocity of the jth mass to the airflow. However, the local incidence of the cable to the flow is based on the $(j-1)$th segment rather than the jth segment. The relative velocity of the cable with respect to the air can be expressed in the rotating frame as follows:

$$\mathbf{v}_j^{\text{rel}} = \mathbf{v}_j - \mathbf{C}_i^r \mathbf{v}_w \tag{A10}$$

where $\mathbf{v}_w$ is the wind velocity expressed in the inertial frame, and $\mathbf{C}_i^r$ is the inertial to rotational direction cosine matrix

$$\mathbf{C}_i^r = \begin{bmatrix} \cos\theta & \sin\theta & 0 \\ -\sin\theta & \cos\theta & 0 \\ 0 & 0 & 1 \end{bmatrix} \tag{A11}$$

The lift and drag coefficients for an inclined cylinder are given by [28]

$$C_{D_j} = C_{f_j} + C_{n_j}\sin^3\vartheta_j \tag{A12}$$

$$C_{L_j} = C_{n_j}\sin^2\vartheta_j\cos\vartheta_j \tag{A13}$$

where the skin friction and crossflow drag coefficients are taken to be [29]

$$C_{f_j} = \begin{cases} 0.038 - 0.0425M_{p_j}, & M_{p_j} < 0.4 \\ 0.013 + 0.0395(M_{p_j} - 0.85)^2, & M_{p_j} \geq 0.4 \end{cases} \tag{A14}$$

$$C_{n_j} = 1.17 + M_{n_j}/40 - M_{n_j}^2/4 + 5M_{n_j}^2/8 \tag{A15}$$

where M_{p_j} and M_{n_j} are the Mach numbers parallel and normal to the jth cable segment, respectively.

The angle of attack of the jth segment may be calculated from

$$\cos\vartheta_j = \frac{-\mathbf{l}_{j-1}\cdot\mathbf{v}_j^{\text{rel}}}{|\mathbf{l}_{j-1}||\mathbf{v}_j^{\text{rel}}|} \tag{A16}$$

The unit vectors defining the directions of the lift and drag vectors are

$$\mathbf{e}_{D_j} = -\frac{\mathbf{v}_j^{\text{rel}}}{|\mathbf{v}_j^{\text{rel}}|} \tag{A17}$$

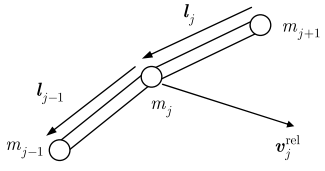

Fig. A1 Definition of cable geometry.

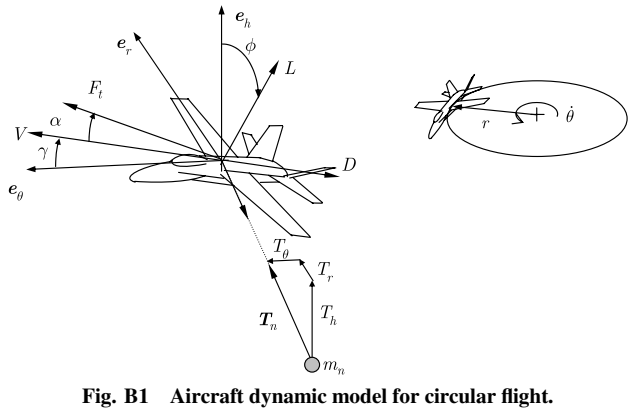

Fig. B1 Aircraft dynamic model for circular flight.

$$\mathbf{e}_{L_j} = -\frac{(\mathbf{v}_j^{\text{rel}}\times\mathbf{l}_{j-1})\times\mathbf{v}_j^{\text{rel}}}{|(\mathbf{v}_j^{\text{rel}}\times\mathbf{l}_{j-1})\times\mathbf{v}_j^{\text{rel}}|} \tag{A18}$$

Hence, the lift and drag vectors may be written as

$$\mathbf{F}_j^{\text{drag}} = \tfrac{1}{2}\rho_j C_{D_j} L_{s_j} d|\mathbf{v}_j^{\text{rel}}|^2\mathbf{e}_{D_j} \tag{A19}$$

$$\mathbf{F}_j^{\text{lift}} = \tfrac{1}{2}\rho_j C_{L_j} L_{s_j} d|\mathbf{v}_j^{\text{rel}}|^2\mathbf{e}_{L_j} \tag{A20}$$

The total aerodynamic force on the jth mass is given by

$$\mathbf{F}_j^a = \mathbf{F}_j^{\text{drag}} + \mathbf{F}_j^{\text{lift}} \tag{A21}$$

The aerodynamic forces on the payload are modeled using a spherical drag model with zero lift,

$$\mathbf{F}_1^{\text{drag}} = -\tfrac{1}{2}\rho_1 C_D A_p|\mathbf{v}_1^{\text{rel}}|\mathbf{v}_1^{\text{rel}} \qquad \mathbf{F}_1^{\text{lift}} = 0 \tag{A22}$$

IV. Gravity Forces

A simple flat Earth model is assumed for the gravity force model such that

$$\mathbf{F}_j^g = -m_j g\mathbf{x}_3 \tag{A23}$$

where g is the acceleration due to gravity at sea level (9.81 m/s^2).

Appendix B: Aircraft Performance Requirements

The performance of an aircraft flying a circular path is affected by the cable tension, and this effect must be accounted for in determining performance requirements for the maneuver. The configuration considered here is shown in Fig. B1. The equations of motion for a point mass aircraft in a circular orbit with a towing cable attached are given by

$$m(\ddot{r} - r\dot{\theta}^2) = -F_t\sin\alpha\sin\phi - \bar{q}SC_L\sin\phi - T_r^{(n)} \tag{B1}$$

$$m(r\ddot{\theta} + 2\dot{r}\dot{\theta}) = (F_t\cos\alpha - \bar{q}SC_D)\cos\gamma - (F_t\sin\alpha\cos\phi + \bar{q}SC_L\cos\phi)\sin\gamma - T_\theta^{(n)} \tag{B2}$$

$$m\ddot{h} = (F_t\cos\alpha - \bar{q}SC_D)\sin\gamma + (F_t\sin\alpha\cos\phi + \bar{q}SC_L\cos\phi)\cos\gamma - mg - T_h^{(n)} \tag{B3}$$

where F_t is the thrust force, α is the angle of attack, ϕ is the bank angle, C_L is the lift coefficient, C_D is the drag coefficient, S is the wing area, γ is the flight path angle, m is the aircraft mass, r is the orbit radius, $\dot{\theta}$ is the angular rate of the aircraft, h is the altitude, g is gravity, and $\bar{q}$ is the dynamic pressure. Note that the direction of the tension vector is taken from the tension applied to the nth lumped mass by the nth cable element. Hence, the tension applied at the aircraft is opposite in direction. The tension components are denoted as $(T_r^{(n)}, T_\theta^{(n)}, T_h^{(n)})$, which are aligned with the $(\mathbf{x}_1, \mathbf{x}_2, \mathbf{x}_3)$ axes when the aircraft lies on the $\mathbf{x}_1$ axis. These nonlinear equations are solved iteratively for the angle of attack, bank angle, and thrust required to maintain circular flight and constant altitude, that is, $\gamma = \dot{r} = \ddot{r} = \ddot{h} = 0$.

Acknowledgment

The first author thanks Pavel Trivailo for supporting some initial work explored in this paper.

References

[1] Chilowsky, C., "Method and Device for Establishing Communication Between Aircraft in Full Flight and the Ground," U.S. Patent 1,829,474, Oct. 1931.

[2] Smith, B. B., "Method and Apparatus for Cargo Loading and Discharging in Flight," U.S. Patent 2,151,395, March 1939.
[3] Anderson, V. R., "Method and Apparatus for Pickup and Delivery by Aircraft in Flight," U.S. Patent 2,295,537, Sept. 1942.
[4] Hitt, R. T., *Jungle Pilot*, Discovery House, Grand Rapids, MI, 1997.
[5] *National Geographic*, Vol. 133, No. 2, Feb. 1968, p. 294.
[6] Simons, J. C., "Long Line Loiter Technique," U.S. Patent 3,724,817, April 1973.
[7] Cotton, R. B., "Aerial Pick-Up and Delivery System," U.S. Patent 3,351,325, Nov. 1967.
[8] Caughey, T. K., "Whirling of a Heavy Chain," *Proceedings of the 3rd U.S. National Congress of Applied Mechanics*, American Society of Mechanical Engineers, New York, 1958, pp. 101–108.
[9] Coomer, J., Lazarus, M., Tucker, R. W., Kershaw, D., and Tegman, A., "A Non-Linear Eigenvalue Problem Associated with Inextensible Whirling Strings," *Journal of Sound and Vibration*, Vol. 239, No. 5, 2001, pp. 969–982.
doi:10.1006/jsvi.2000.3190
[10] Lemon, G., and Fraser, W. B., "Steady-State Bifurcations and Dynamical Stability of a Heavy Whirling Cable Acted on by Aerodynamic Drag," *Proceedings of the Royal Society of London A*, Vol. 457, No. 2009, 2001, pp. 1021–1041.
doi:10.1098/rspa.2000.0704
[11] Skop, R. A., and Choo, Y.-I., "The Configuration of a Cable Towed in a Circular Path," *Journal of Aircraft*, Vol. 8, No. 11, 1971, pp. 856–862.
doi:10.2514/3.44310
[12] Russell, J. J., and Anderson, W. J., "Equilibrium and Stability of a Whirling Rod-Mass System," *International Journal of Non-Linear Mechanics*, Vol. 12, No. 2, 1977, pp. 91–101.
doi:10.1016/0020-7462(77)90028-2
[13] Russell, J. J., and Anderson, W. J., "Equilibrium and Stability of a Circularly Towed Cable Subject to Aerodynamic Drag," *Journal of Aircraft*, Vol. 14, No. 7, 1977, pp. 680–686.
doi:10.2514/3.58840
[14] Zhu, F., and Rahn, C. D., "Stability Analysis of a Circularly Towed Cable-Body System," *Journal of Sound and Vibration*, Vol. 217, No. 3, 1998, pp. 435–452.
doi:10.1006/jsvi.1998.1782
[15] Cohen, Y., and Manor, H., "Equilibrium Configurations of a Cable Drogue System Towed in a Helical Motion," *International Journal of Engineering Science*, Vol. 26, No. 8, 1988, pp. 771–786.
doi:10.1016/0020-7225(88)90029-8
[16] Zhu, F., Hall, K., and Rahn, C. D., "Steady State Response and Stability of Ballooning Strings in Air," *International Journal of Non-Linear Mechanics*, Vol. 33, No. 1, 1998, pp. 33–46.
doi:10.1016/S0020-7462(96)00154-0
[17] Williams, P., and Trivailo, P., "Dynamics of Circularly Towed Aerial Cable Systems, Part I: Optimal Equilibrium Configurations and Their Stability," *Journal of Guidance, Control, and Dynamics*, Vol. 30, No. 3, 2007, pp. 753–765.
doi:10.2514/1.20433
[18] Williams, P., and Trivailo, P., "Dynamics of Circularly Towed Aerial Cable Systems, Part II: Transitional Flight and Deployment Control," *Journal of Guidance, Control, and Dynamics*, Vol. 30, No. 3, 2007, pp. 766–779.
doi:10.2514/1.20434
[19] Williams, P., and Trivailo, P., "Periodic Solutions for Cable-Body Systems Towed in Circular and Elliptical Paths," AIAA Paper 2006-6374, Aug. 2006.
[20] Williams, P., "Periodic Optimal Control of a Towed Aerial-Cable System in Presence of Cross-Wind," AIAA Paper 2006-6192, Aug. 2006.
[21] Williams, P., and Trivailo, P., "Cable-Supported Sliding Payload Deployment from a Circling Fixed-Wing Aircraft," *Journal of Aircraft*, Vol. 43, No. 5, 2006, pp. 1567–1570.
doi:10.2514/1.21132
[22] Borst, R. G., Greisz, G. F., and Quynn, A. G., "Fuzzy Logic Control Algorithm for Suppressing E-6A Long Trailing Wire Antenna Wind Shear Induced Oscillations," AIAA Paper 93-3868, Aug. 1993.
[23] Brushwood, D. L. J., Olson, A. P., and Smyth, J. M., "The E-6A Orbit Improvement System and Its Effect Upon LTWA Verticality," AIAA Paper 98-4426, Aug. 1998.
[24] Alabrune, F., "Art of Aerial Transportation," U.S. Patent 2,298,912, Oct. 1942.
[25] Alabrune, F., "Transportation Method," U.S. Patent 2,373,086, April 1945.
[26] Wilson, F. M., "Aerial Transport of Payloads with Vertical Pick Up and Delivery," U.S. Patent 4,416,436, Nov. 1983.
[27] Williams, P., "Towing and Winch Control Strategy for Underwater Vehicles in Sheared Currents," *International Journal of Offshore and Polar Engineering*, Vol. 16, No. 3, 2006, pp. 218–227.
[28] Hoerner, S. F., *Fluid-Dynamic Drag*, published by the author, Bakersfield, CA, 1965.
[29] Cochran, J. E., Innocenti, M., No, T. S., and Thukral, A., "Dynamics and Control of Maneuverable Towed Flight Vehicles," *Journal of Guidance, Control, and Dynamics*, Vol. 15, No. 5, 1992, pp. 1245–1252.
doi:10.2514/3.20975